Supplementary Information

Activate Capture and Digital Counting (AC+DC) assay for protein biomarker detection integrated with a self-powered microfluidic cartridge

Congnyu Che[a], Nantao Li[b], Kenneth D. Long[a], Miguel Angel Aguirre[c], Taylor D. Canady[d], Qinglan Huang[b], Utkan Demirci[e], and Brian T. Cunningham[a,b,d,*]

a. Department of Bioengineering, University of Illinois at Urbana-Champaign, 208 North Wright Street, Urbana, IL 61801, USA

b. Department of Electrical and Computer Engineering, University of Illinois at Urbana-Champaign, 208 North Wright Street, Urbana, IL 61801, USA

c. Department of Analytical Chemistry and Food Science and University Institute of Materials, Faculty of Science, University of Alicante, 03080 Alicante, Spain

d. Carl R. Woese Institute for Genomic Biology, University of Illinois at Urbana-Champaign, 1206 West Gregory Drive, Urbana, IL 61801, USA

e. Bio-Acoustic MEMS in Medicine (BAMM) Laboratory, Canary Center at Stanford for Cancer Early Detection, Department of Radiology School of Medicine Stanford University, Palo Alto, CA 94304, USA

1. Resonant reflection spectrum of the PC biosensor

The resonant reflection spectrum from one pixel of a PRAM image is shown in Supplementary Figure 1 with and without an attached gold nanoparticle (AuNP), indicating a reflected intensity reduction of 22% when the AuNP is observed.

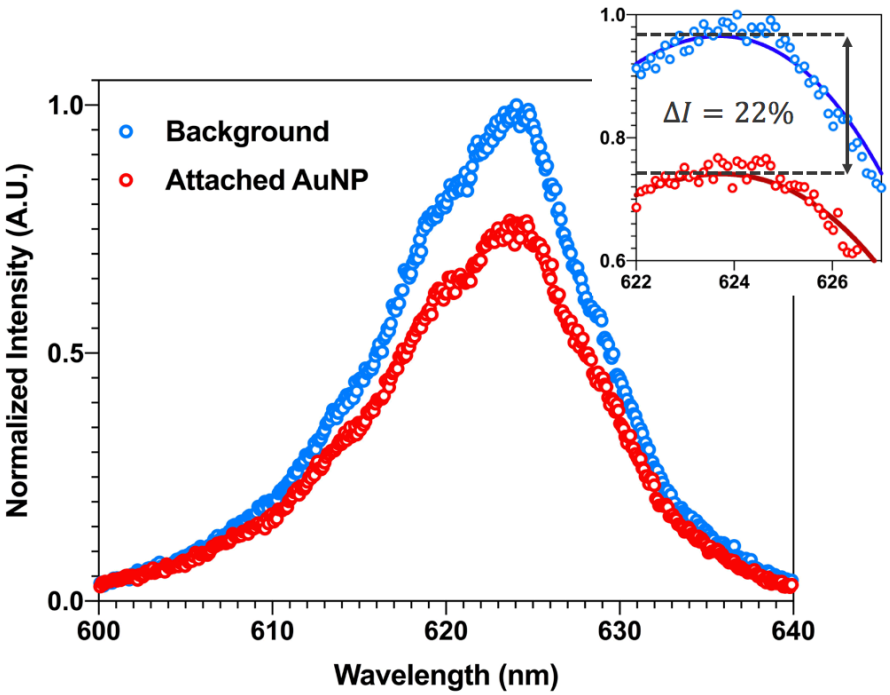

Supplementary Figure 1. Example spectrum with a reflected intensity change with/without an attached AuNP. Inset: Zoomed in image of the normalized spectrum with third order polynomial fitting (background fitting in blue line, AuNP fitting in red line).

2. AuNP patterns on the PRAM image

The elongated patterns observed on the PRAM images originate from the non-uniform enhanced field on the photonic crystal (PC) surface. Specifically, the PC grating periodicity is oriented in the vertical direction in our images, and thus the PC resonant electromagnetic field intensity is periodic in the horizontal direction, while uniform in the vertical direction. The periodic illumination patterns shifts the center of the Fourier plane towards higher frequencies,[1] resulting in the observed side lobes in the image, surrounding each surface-bound AuNP on its left and right sides. In addition, the vertical distance between the nanoparticle and the PC surface can induce either a reduced intensity or an increased intensity at the central location of the AuNP. While this

topic is outside the scope of the present manuscript, a brief description of this phenomenon is as follows: AuNPs attached to the PC with a vertical separation distance of several nanometers induce efficient quenching the PC resonant electromagnetic field, and thus we observe a prominent dark spot in the reflected intensity from the location at which the AuNP is present. However, depending upon the precise orientation of the capture antibody on the AuNP and the secondary antibody on the PC, it is possible that the proteins will displace the AuNP in the vertical direction by ~30-50 nm. Numerical simulations of vertically displaced AuNPs reveals that this situation leads to constructive interference between light scattered by the AuNP and the reflected light from the PC structure, resulting in the greater intensity at the center of the AuNP, as demonstrated in Supplementary Figure 2.[2] This phenomenon opens the potential for utilizing the PRAM intensity to measure vertical displacements of single biomolecular interactions, which is an interesting topic outside the scope of this work. Here, we count both dark-centered and bright-centered AuNP patterns to generate our quantitative assay output.

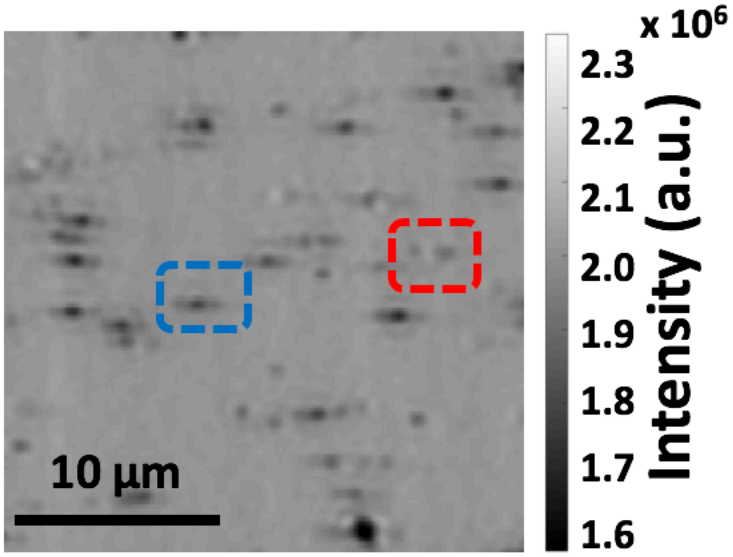

Supplementary Figure 2. PRAM image of AuNPs. The AuNP patterns are composed of two side lobes with either bright center (red dashed box), or a dark center (blue dashed box).

3. AuNP-IgG conjugation solution

The IgG conjugated AuNP (AuNP-IgG) solution was prepared by adding 12 µL of SH-PEG-IgG solution to 200 µL of stock AuNP solution. The SH-PEG-IgG solution was added in a series of small volumes (4µL), and the hydrodynamic diameter of AuNU-IgG conjugates was were measured by Dynamic Light Scattering (model DelsaMax Pro, Beckman Coulter, Pasadena, CA, USA). Figure 3 shows the hydrodynamic diameter of AuNPs in solution before and after adding incremental volumes of SH-PEG-IgG. 12 µL of SH-PEG-IgG was selected to ensure optimal bioconjugation, representing the point at which AuNPs reached their binding capacity.

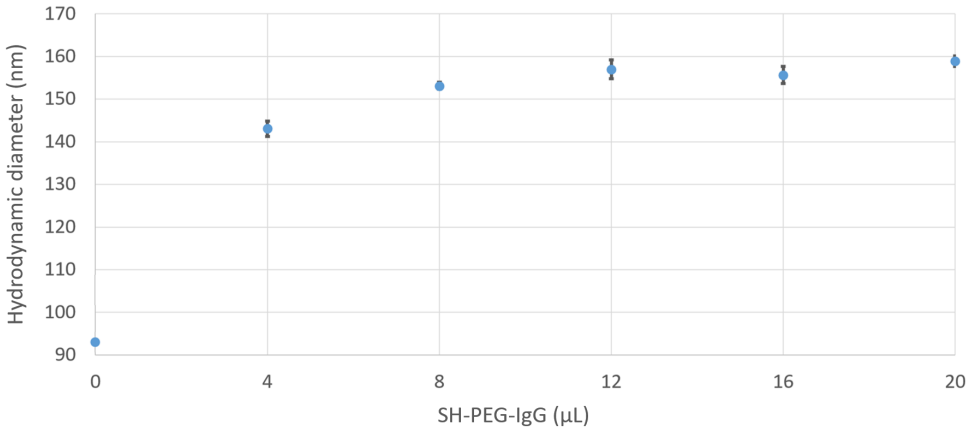

Supplementary Figure 3. Relationship between hydrodynamic diameter of AuNPs in solution and the volume of SH-PEG-IgG, used to determine conditions that result in full occupancy of binding for IgG on the AuNP surface.

4. COMSOL simulation parameters and governing equations

We demonstrate a 2-D cross-section model to simulate the transport and adsorption of biomolecules on the PC biosensor embedded in the microfluidic cartridge. The Transport of Diluted Species (tds) and the General Form Boundary PDE (gb) physics are coupled together to

solve this mass balance problem. The parameters involved in this simulation are shown in Table 1. The mass balance for the PC biosensor surface, including surface diffusion and the reaction rate expression for the generation of the absorbed AuNPs, C_s, is:

$$\frac{\partial C_s}{\partial t} + \nabla \cdot (-D_s \nabla C_s) = k_{on} c(\Gamma_s - c_s) - k_{off} c_s \quad (1)$$

Where D_s is the surface diffusivity, and Γ_s is the total surface concentration of the active sites. With the coupling between two mass transfer mechanisms (diffusion and surface adsorption), we define the boundary conditions of the AuNPs transport in the microfluidic channel as:

$$c = c_0 \quad \text{at the inlet} \quad (2)$$

$$\vec{n} \cdot (-D\nabla \mathrm{c} + \mathrm{c}\vec{u}) = 0 \quad \text{at the microfluidics channel walls and inactivated sites} \quad (3)$$

$$\vec{n} \cdot (-D\nabla \mathrm{c} + \mathrm{c}\vec{u}) = -k_{on} c(\Gamma_s - c_s) + k_{off} c_s \quad \text{at the PC biosensor active area} \quad (4)$$

$$\vec{n} \cdot (-D\nabla \mathrm{c} + \mathrm{c}\vec{u}) = \vec{n} \cdot \mathrm{c}\vec{u} \quad \text{at the outlet} \quad (5)$$

Where $\vec{n}$ is the unit normal vector directed out of a surface, and $\vec{u}$ is the velocity of the fluid. Boundary condition (2) constrains the AuNP solution injected into the channel to have constant concentration c_0. Boundary (3) ensures that no AuNP can diffuse out of the channel walls. Boundary condition (4) describes the binding kinetics at the PC active area, considering the rate of the reaction at the active area, the flux of the AuNPs, and the concentration of absorbed AuNPs.

Table 1. Parameters for COMSOL 2-D model

Name	Value	Description
C_o	1.66×10^{-17} mol L^{-1}	Initial concentration of AuNPs
k_{on}	1×10^{6} M^{-1} s^{-1}	Typical value for k_{on}
k_{off}	1×10^{-5} s^{-1}	Typical value for k_{off}
b_{max}	2×10^{-8} kg m^{-2}	Active site concentration
D_s	1×10^{-11} m^2 s^{-1}	Surface diffusivity
D	3.8×10^{-12} m^2 s^{-1}	AuNPs diffusivity

H	2.5×10^{-5} m	Channel height
W_c	5×10^{-4} m	Channel width
L	9×10^{-3} m	Channel length
V_{max}	0.0018 m s^{-1}	Maximum velocity

5. Explanation for the nonlinearity of the p24 dose-response curve

When the test sample contains extremely low concentrations of p24, the ratio of p24 to AuNP is small (typically << 1:1), and the percentage of activated AuNPs that bind with p24 molecules follows a Poisson distribution.[3] In this case, the Poisson statistics predict that the expected average number of p24 molecules per AuNP becomes exceptionally low, the distribution is extremely narrowed, so in most cases each AuNP carries either a single p24 molecule or none. For example, in our protocol, when we mix the same volume of the 10 pg mL^{-1} (0.4 pM) p24 and the AuNP conjugate (4.5 pM) solution, then 10% of the AuNPs will carry one p24 protein molecule and 90% will not carry any protein molecules. Thus, at low concentrations, the relationship between captured AuNPs and the number p24 molecules is approximately linear. When the concentration of p24 increases beyond 100 pg mL^{-1}, one AuNP is more likely to bind with multiple p24 molecules. In this case, the expected average number of p24 molecules per AuNP becomes larger, the distribution is broader, each AuNP may carry 0 to 10 (each AuNP has approximately ten binding sites) p24 molecules. Thus, the relationship between the number of captured AuNPs and the number of p24 molecules becomes sublinear towards high concentrations. Furthermore, when the concentration of p24 molecules continues increasing (higher than 1 ng mL^{-1}), it is possible that a majority of the binding sites on AuNPs will be occupied, and consequently p24 molecules will be unbound in the sample. As the sample flows across the PC surface, these remaining molecules

would have the opportunity to occupy the limited binding sites on the PC and block the binding between AuNPs and the immobilized antibodies on the PC.

According to prior studies that utilize capture of target analytes upon a fixed number of particles, the percentage of activated AuNPs that bind with p24 molecules follows a Poisson distribution: $P(X = k) = \frac{\lambda^k e^{-\lambda}}{k!}$.[3] In our case, k is the discrete random variable representing the number of p24 molecules bound to a single AuNP, and λ is the expected value of k. To establish the Poisson distribution for each p24 concentration, we know the average number of captured AuNPs, which is the average count of AuNPs/mm^2 in Figure 5b multiplied by the sensing area of the PC sensor. Although the capture efficiency changes with respect to the concentration of activated AuNPs, we can estimate the capture efficiency for various p24 concentrations using our measurements of pre-activated AuNPs from Figure 4c. Then, we are able to obtain the number of activated AuNPs (number of captured AuNPs divided by capture efficiency) and the percentage of activated AuNPs, which is $1 - P(X = 0)$. Since $P(X = 0) = e^{-\lambda}$, we can calculate the expected number of p24 molecules on AuNPs, which we then multiply with the total number of AuNPs in the sample. Thus, we can estimate the total number of p24 molecules bound across all AuNPs in the sample based on the Poisson distribution (Calculations are shown in Table 2). With this information, we can plot a Poisson-corrected dose-response curve, shown in Supplementary Figure 4. In this figure, the y-axis is the expected total number of bound p24 molecules distributed across all AuNPs in the sample, based on the measurements. The x-axis is the true concentration of p24 molecules in the test sample. Figure 4 demonstrates a linear relationship for the lower concentrations and then reaches a plateau at the highest concentration. The saturation originates from the fact that, as shown in Table 2, Column B, for a fixed number of AuNPs, increasing the p24 concentration results in a sub-linear increase in the number of activated AuNPs, as more than one p24 will likely

bind with each AuNP. As the fraction of activated AuNPs approaches 40%, there is an expected diminishing return in AC+DC "counted" AuNPs.

Table 2. Calculation of the total number of bound p24 molecules, based on the measurements

	Column A	Column B	Column C	Column D
Concentration of p24 (g/mL)	**Estimated # of activated AuNPs**	**% of activated AuNPs (%)**	**p24/AuNP ratio from Poisson**	**Total # of p24 on 5.37×10^7 AuNPs**
1×10^{-12}	590163	1.10	0.011	5.2×10^5
1×10^{-11}	2444444	4.55	0.047	2.5×10^6
1×10^{-10}	15030303	27.99	0.328	1.8×10^7
1×10^{-9}	19600000	36.50	0.454	2.4×10^7

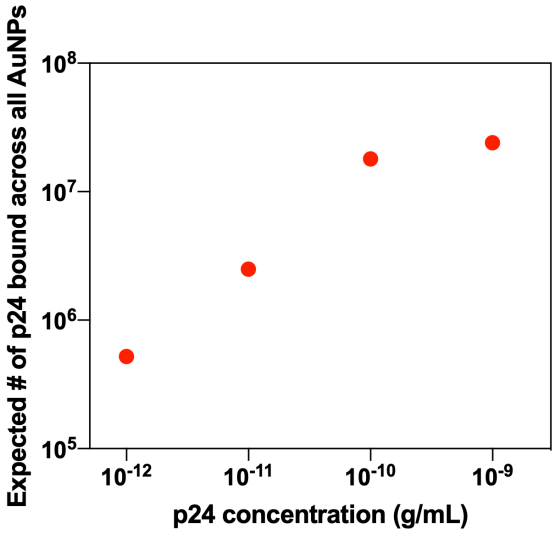

Supplementary Figure 4. Relationship between the true p24 concentration and the calculated total number of p24 bound (distributed across all 5.37×10^7 AuNPs, Column D in Table 2). This amount is determined by multiplying "p24/AuNP ratio from Poisson" (Column C in Table 2) with 5.37×10^7 AuNPs in the sample. The Poisson-corrected dose-response curve demonstrates a linear increase at low concentrations and a plateau at the highest concentration.

References

1. Wei F, Liu Z. Plasmonic structured illumination microscopy. Nano Lett. 2010;10(7):2531-6.
2. Sevenler D, Daaboul GG, Ekiz Kanik F, Unlu NL, Unlu MS. Digital Microarrays: Single-Molecule Readout with Interferometric Detection of Plasmonic Nanorod Labels. ACS Nano. 2018;12(6):5880-7.
3. Rissin, D.M. and D.R. Walt, *Digital Concentration Readout of Single Enzyme Molecules Using Femtoliter Arrays and Poisson Statistics.* Nano Letters, 2006. **6**(3): p. 520-523.